Retrieval of CO from nadir remote-sensing measurements in the infrared using four different inversion algorithms

Cathy Clerbaux, Juliette Hadji-Lazaro,

Service d'Aéronomie, Paris, France

ccl@aero.jussieu.fr

Sébastien Payan, Claude Camy-Peyret,

Laboratoire de Physique Moléculaire et Applications, Paris, France

Jinxue Wang, David P. Edwards,

National Center for Atmospheric Research, Boulder, Colorado

Ming Luo

Jet Propulsion Laboratory, Passadena, California

Four inversion schemes based on various retrieval approaches (digital gas correlation, non-linear least squares, global fit adjustment, and neural networks) developed to retrieve CO from nadir radiances measured by different downward looking satellite-borne instruments (MOPITT, TES, IASI) were compared both for simulated cases and for atmospheric spectra recorded by the IMG instrument. The sensitivity of the retrieved CO total column amount to parameters that may impact the inversion accuracy (noise, ancillary temperature profile and water vapor content) was investigated. The CO column agreements for the simulated radiance spectra were within 4%, whereas larger discrepancies were obtained when atmospheric spectra recorded by the IMG instrument were analyzed. The assumed vertical temperature profile is shown to be a critical parameter for an accurate CO retrieval. The instrument line shape was also identified as a possible cause of disagreement between the results provided by the participating groups. © 2002 Optical Society of America

OCIS codes: 010.1280,010.7030,280.1120,300.6300,300.6340

1. Introduction

During recent decades, the impact of human activities on the chemical composition of the atmosphere and global warming of climate has been the subject of increasing worldwide concern.[1,2] In the near future, satellite data will represent the majority of the observations available to improve our understanding of global tropospheric chemistry. As a precursor of the production of ozone (O_3) and as the leading sink of hydroxyl radical (OH), carbon monoxide (CO) is one of the key tropospheric trace species that need to be measured on the global scale. The primary emission sources of CO are

associated with technological processes (transport, combustion, and industrial activities), biomass burning, biogenic sources and oceans. Secondary sources come from the oxidation of methane (CH_4) and non-methane hydrocarbons (NMHC). Huge uncertainties remain on the estimated strengths of both natural and anthropogenic sources.[1] The chemical lifetime of CO varies from less than one month in the tropics to several months in the polar regions during winter, leading to large spatial and temporal variability of the CO global distribution. The analysis and interpretation of data measured by space-borne nadir-looking instruments provide valuable information to study the CO sources, sinks and transport processes.

The first CO tropospheric measurements from space were performed by the Measurement of Air Pollution from Satellites (MAPS) experiment, a gas correlation spectrometer carried onboard the Space Shuttle during limited time periods. CO retrievals were obtained for November 1981,[3] October 1984,[4] April and October 1994.[5,6] Stratospheric and upper tropospheric CO measurements were also provided between 26-31^{o}N and 46-48^{o}S by the Atmospheric Trace Molecular Spectroscopy (ATMOS) Fourier transform spectrometer during the Spacelab 3 Shuttle mission in May 1985.[7] The Interferometric Monitor for Greenhouse Gases (IMG) instrument flew aboard the Japanese Advanced Earth Observing System (ADEOS) from August 1996 to June 1997 and provided the first high resolution (0.1 cm^{-1}) Fourier transform infrared spectra in the nadir geometry.[8,9] More recently (December 1999), the Measurements Of Pollution In The Troposphere (MOPITT) instrument[10] was launched as part of NASA's EOS-TERRA payload and has already given promising information on the tropospheric abundance of CO.[11,12]

Other nadir-viewing instruments that observe the spectrum of the Earth's atmosphere in the thermal infrared spectral range are planned for launch to probe the troposphere from polar-orbiting satellites. In the coming years, the Atmospheric InfraRed Sounder (AIRS)[13] will be launched on the US EOS-AQUA platform, the Tropospheric Emission Spectrometer (TES)[14] is due to fly on

EOS-AURA, and the Infrared Atmospheric Sounding Interferometer (IASI)[15] will be carried by the European METOP series of satellites. In order to maximize the scientific return to be expected from these missions, efforts are being dedicated towards the development of fast forward radiative codes and efficient Level2 (L2) inversion methods for the retrieval of infrared absorbing trace species.

2. Methodology and aims of the intercomparison

Intercomparison experiments are needed to validate the information that can be measured from a remote-sensing instrument. Several *in situ* comparison campaigns that gathered different kinds of instruments measuring atmospheric concentrations for several compounds at the same time and at the same geographical location have been organized.[16,17] Each instrument can use a different measurement technique, with an associated software (the so-called retrieval algorithm) to extract the desired information (in this case atmospheric abundances for trace gases) from the raw data. A retrieval algorithm generally relies on a forward radiative transfer code, a spectroscopic database, and a minimization scheme.

As different nadir-sounding infrared instruments, all able to provide CO measurements on the global scale, could potentially fly during the same time period, it was found interesting to compare the L2 retrieval algorithms currently developed at National Center for Atmospheric Research (NCAR) for MOPITT, at Jet Propulsion Laboratory (JPL) for TES, and at Laboratoire de Physique Moléculaire et Applications (LPMA) and Service d'Aéronomie (SA) for IASI.

This paper is not intended as a comprehensive presentation of existing inversion methods, but aims at comparing the performance of different inversion algorithms on a common set of data, in order to quantify the level of agreement obtained when retrieving CO total column abundances and to investigate on the possible causes of discrepancies. In 1999, high-resolution nadir radiance spectra

measured in the thermal infrared spectral range were available from the IMG measurements, allowing the four groups to test their algorithms on real atmospheric spectra. The algorithms used different forward radiative transfer codes, different minimization schemes, but a common spectroscopic database.[18] As line-by-line forward radiative codes intercomparison exercises were already reported in the literature,[19,20] we focused on inversion codes that are specific to each instrument. Inversion of geophysical parameters from remotely sensed observations is well known to be a ill-posed problem.[21] A variety of methods exists for the retrieval of atmospheric profiles from the spectra measured by remote sounders. A large body of literature is available on the subject,[22–24] and the most widely used approaches in atmospheric remote sensing are described in [Rodgers, 2000].[25] Retrievals of trace gas and temperature profiles in the thermal infrared spectral range were reported both for simulation studies[26–28] and airborne experiments.[29,30] The accuracy of the retrieved quantities and the ability to retrieve low-resolution vertical profiles from the data provided by an instrument partly rely on the efficiency of the inversion procedure.

The L2 inversion codes used in this study are continually evolving to improve efficiency and performance. The 1999 version of each algorithm was used for this exercise, and data were not reprocessed with improved versions that have become available since then. All schemes were not at the same level of maturity, and some needed adaptation to be able to analyze IMG spectra. Each group was provided with a set of cloud-free IMG data, along with a set of synthetic spectra simulated using the IMG characteristics to investigate the impact of different parameters that may affect the CO retrieval, in order to help analyze the results.

This manuscript summarizes the results and discusses the agreement obtained for CO total column retrievals from a common dataset. The paper is organized as follows: First, we briefly describe the inverse problem and the retrieval schemes that were used in the intercomparison exercise (Section 3). Next, sensitivity studies to assess the performance of the four algorithms with regard to

parameters that may have an impact on the retrieval accuracy are reported, as well as CO inversion results from atmospheric spectra recorded by the IMG instrument (Section 4). In Section 5 we conclude with recommendations for improved CO retrievals for forthcoming instruments.

3. Retrieval methods

A. Inverse problem

The general remote sensing equation can be written, in a schematic form, as[25]

$$\mathbf{y} = \mathbf{F}(\mathbf{x}, \mathbf{b}) + \epsilon$$

where $\mathbf{y}$ is the measurement vector (here the measured infrared radiances), and $\mathbf{F}(\mathbf{x}, \mathbf{b})$ is the forward model function. $\mathbf{x}$ is the state vector (here the CO concentration to be inferred from the measurement), and $\mathbf{b}$ represent all other parameters used in the forward model: pressure, temperature, other constituent profiles, surface emissivity, instrument spectral function, and spectroscopic parameters. ϵ is the measurement error due to instrumental noise.

The inverse problem consists in retrieving $\mathbf{x}$ for a given $\mathbf{y}$. For nadir-looking measurements, this problem is known to be non-linear and under-constrained as components of the atmospheric vertical profile do not contribute to the measurements and hence can not be detected. The solution is non-unique and is generally unstable. As mentioned in Section 2, different statistical and regularization techniques exist to derive a valid solution,[25] allowing a priori knowledge or statistical (climatology) information to be taken into account.

B. Retrieval schemes

The L2 inversion methods employed in this comparison exercise use different forward radiative codes, with different spectral ranges and minimization algorithms for the CO retrieval. Associated computing speed is variable according to the number of simultaneously retrieved species. A short

description of each algorithm is provided hereafter, and Table 1 summarizes their main characteristics. The reader is invited to read the referenced publications for an extended description of each algorithm.

1. NCAR inversion algorithm

The MOPITT retrieval code is based on a parameterized fast forward model[31] and uses the maximum likelihood inversion method.[32]The Digital Gas Correlation (DGC) retrieval technique,[33,34] specifically developed to integrate observations made by different instruments (IMG, TES), was used for this intercomparison exercise. The simulated radiances and IMG spectra to be inverted were synthesized into MOPITT-like signal (thermal channels only) by filtering the spectra with the MOPITT instrument function.[35]

2. JPL inversion algorithm

The JPL TWPR (Tes Working Prototype Retrieval) algorithm, developed by the TES science team for TES Level2 retrievals, is described in the TES Level2 Algorithm Theoretical Basis Document (ATBD).[36] The general retrieval approach is to use non-linear least squares spectral fitting based on the so-called optimal estimation technique.[25] For computational efficiency, a table of look-up absorption coefficients at pre-defined pressure and temperature sets, and analytical Jacobian calculation are used in the forward model. The code can accommodate both profile and column abundance retrievals.[37]

3. LPMA inversion algorithm

The LPMA retrieval algorithm is composed of an accurate radiative transfer model and an efficient minimization algorithm of the Levenberg-Marquardt type.[38] The global fit method[39] is used, allowing simultaneous retrieval of the column amounts of more than 8 species, surface temperature, surface emissivity, and instrumental spectral response function from a radiance spectra. For the

present work, the algorithm was tailored to the specifics of the IMG spectra and geometry.[40]

4. SA inversion algorithm

The SA retrieval scheme is based on a multilayer neural network that uses a gradient descent back-propagation algorithm.[40,41] Neural network techniques allow the solution of regression problems by estimating a transfer function from a set of known situations which constitutes the a priori information necessary to solve the problem. The database used to train the network was built from atmospheric concentration profiles calculated by a 3D chemical-transport model,[42] coupled to a radiative transfer code and convoluted with the desired instrumental function.[43]

4. CO inversion

A. Simulated radiance spectra

Preliminary results obtained to compare the CO retrieval performance using the NCAR, LPMA and SA codes on infrared nadir spectra were previously reported.[44] Concurrently with the analysis of CO inversion from the IMG atmospheric spectra, it was found necessary to perform sensitivity studies on simulations of IMG data, to study how errors associated with other parameters could propagate in the retrieved CO column amount. The spectrum of infrared radiation emitted by the Earth's surface and absorbed by the atmosphere as recorded by the IMG instrument in the nadir geometry was calculated using a high-resolution line-by-line radiative transfer code[45] with the HITRAN96 spectroscopic database.[18] CO concentration and temperature profiles (plotted in Figure 1) extracted from the 3-D chemistry-transport MOZART model[46,47] simulations above North Atlantic Ocean (50^{o}N, 25^{o}E) for summer conditions were used as input, along with the Air Force Geophysics Laboratory (AFGL) U.S. Standard Atmosphere 1976 standard concentration profiles for other absorbing species (H_2O, N_2O, O_3 and CH_4). Surface emissivity was set to one. Solar ground reflection was not included in the calculation. The upwelling radiances were calculated on

48 fixed altitude levels from surface to 120 km. The high-resolution ($5x10^{-4}$ cm^{-1}) spectrum calculated between 2000 and 2500 cm^{-1} was then re-sampled and convoluted to simulate IMG Level 1C radiance channels. The spectral dispersion of IMG in the CO absorption spectral range was set to 0.040177 cm^{-1}. As the exact IMG instrument line shape (ILS) was unavailable, we used a Norton-Beer weak apodization function (full width at half maximum=0.06909 cm^{-1}) as our investigations showed that the unapodized IMG Level 1C data around 2100 cm^{-1} can be reasonably fitted using this function.[48] Figure 2 (top) illustrates the radiative transfer simulation for IMG conditions, used hereafter as the reference (unperturbed) case. This radiance spectrum contains intense absorption features due to rovibrational transition lines from the 1-0 CO fundamental band between 2030 and 2230 cm^{-1}, with well-resolved lines associated with R and P branches (see Figure 2 bottom). Interferences with absorption features of H_2O, CO_2, O_3 and N_2O occur.

As described in Section 2, radiances recorded by an infrared nadir-looking instrument are a function of trace gas concentrations, atmospheric temperature profile, surface emissivity, and instrumental characteristics (noise and resolution). Other parameters like clouds or aerosols may also affect the measurement. For cloud-free conditions, most of the uncertainty on the retrieved quantities comes from the instrumental noise, and the use of a temperature or other constituent vertical profile that may be erroneous. The sensitivity of the retrieved CO total column amounts to the following parameters has then been investigated: (1) instrumental noise, (2) temperature profile, (3) water vapor content.

1. Instrumental Noise

In order to simulate the contribution of the instrumental noise to the signal, the reference radiance spectrum was perturbed using a Gaussian random number generator. The standard deviation of the noise level was set to $2x10^{-5}$ $W/m^2cm^{-1}sr$, corresponding to the IMG associated noise for the

2100 cm^{-1} spectral range.

2. Temperature profile

Temperature profiles are usually retrieved from the rovibrational bands of CO_2 around 650-700 cm^{-1}. For the forthcoming high spectral resolution instruments, it is expected that temperature will be measured with an accuracy of 1 K (RMS) at a vertical resolution of 1 km, at least in the lower troposphere. The use of an erroneous temperature profile in the inversion process directly impacts the retrieval accuracy.

To simulate a realistic erroneous temperature profile, we used an error covariance matrix provided by Meteo-France which characterizes the accuracy associated with the retrieval of a temperature profile for the IASI instrument. A previous example of such a matrix, which contains both diagonal and off-diagonal elements, was provided in [Clerbaux et al.,[43] see Figure 6]. The initial temperature profile was randomly perturbed using this error covariance matrix. Both the initial and the perturbed temperature profiles are plotted in Figure 1. Differences are about 0.5 K at surface level (T_s), between 0.05 K and 1 K from surface to 7 km, between 0.5 K and 5 K from 7 km to 18 km, and increase at higher altitudes.

3. H_2O profile

H_2O is the main interfering constituent in the CO absorption spectral range, with numerous absorption lines spread throughout the spectrum. The interferences due to other constituents (N_2O, CO_2 and O_3) are easier to get rid of by careful selection of the microwindows used in the inversion process. To study how uncertainties on H_2O impact the signal, a random perturbation of 10% (which is the expected accuracy to be provided by forthcoming infrared sensors) was applied to the initial H_2O profile.

4. Results

Four specific radiance simulation cases combining these three sources of error were prepared. Radiance perturbations from the initial unperturbed reference case are plotted in Figure 3: cases A, B, C and D are associated with the radiance contribution due to the noise perturbation, the temperature profile perturbation, the combined noise and temperature perturbation, and the H_2O perturbation, respectively. The reference spectrum and the four perturbed spectra were distributed to each participating group, along with the ancillary data (temperature and other constituent profiles) associated with the unperturbed reference case, but without information on which specific parameter was investigated each time. The CO total column inversion results (CO_{inv}) obtained from each group are represented in Figure 4. For the sake of clarity, and as this part of the exercise was focused on the study of how the various parameters affect the CO retrieved values, the results are plotted as relative deviations from the reference case (CO_{ref}), in %: (CO_{inv}-CO_{ref})x100/CO_{ref}. For each participant, CO_{ref} corresponds to the CO amount retrieved from the unperturbed radiance spectrum. For JPL and LPMA, two sets of results were provided for each case, one set with fixed surface temperature at the value initially provided, and a second set allowing for the surface temperature to be adjusted by the fitting procedure. The results provided by NCAR are with fitted surface temperature. The SA algorithm is working with relative radiance values (baseline subtracted) to overcome the surface temperature adjustment.

When analyzing these results in detail, it can be seen that for all the groups the addition of noise induces a small (null, slightly negative or positive, but always lower than 4%) contribution to the retrieved CO value (case A). The algorithms have different degrees of sensitivity when using a different temperature profile in the inversion process than the one that was used to generate the spectrum (case B). When the provided surface temperature parameter (which indeed differed by 0.5 K from the true surface temperature) was not adjusted by the fitting procedure, discrepancies

of 40 % can be reached. Conversely, when allowing this parameter to be fitted, the agreement on CO retrievals among the different groups reached 3 %. Case C for which both noise (same noise used as for case A) and a different temperature (same as for case B) were combined is consistent with the results obtained for these two cases. Finally, the use of a perturbed H_2O profile does not show a significant impact on the retrieval for all the groups (case D). In summary, when surface temperatures were allowed to be adjusted, relative agreements better than 4% were found between the different codes for all four simulated cases corresponding to perturbed situations. These differences are to be compared to the 10% accuracy value which is expected for the CO column amount retrieved from nadir infrared radiances. From this part of the comparison exercise, we concluded that all four algorithms proved to be robust to the noise contribution and to the retrieval errors due to imperfect knowledge of temperature and H_2O profiles, at least for reasonable noise level and moderately perturbed profiles as those used for this part of the study.

B. IMG radiance spectra

1. IMG instrument

The IMG instrument[8,9] operated on board the ADEOS satellite and provided 10 months of data until the breakdown of the platform solar panel. IMG was a nadir-viewing Fourier transform interferometer that recorded the thermal emission of the Earth-atmosphere system between 600 and 3030 cm^{-1}, with a maximum optical path difference (OPD) of 10 cm. Owing to the polar orbit of the satellite, the instrument provided a global coverage of the Earth, making $14\frac{1}{4}$ orbits per day with series of six successive measurements separated by 86 km along the track, followed by the observation of deep space and of an internal blackbody for calibration purposes. The footprint on the ground was 8 km x 8 km, in three spectral bands (band 1 from 2387 to 3030 cm^{-1}, band 2 from 2000 to 2500 cm^{-1}, and band 3 from 600 to 2000 cm^{-1}), corresponding to three different detectors and three geographically adjacent footprints. The availability (through IMGDIS/ERSDAC) of the

Level 1C atmospheric data recorded by the IMG instrument allowed us to compare our retrieval schemes on real atmospheric data.

2. Results

A set of five spectra (referred hereafter as img304, img307, img822, img906, img921) recorded at different places of the world and at different time of the year, was selected from the available IMG atmospheric data (version 5.5.2.3), each having already been documented as cloud-free data in previous papers.[35,40,49] Table 2 summarizes the time and location for each studied IMG spectrum. The calibrated IMG Level 1C data are available with quality flags, associated with three separate criteria: quality of the interferogram, quality of the alignment, and phase difference.[9] We checked that all five selected cases corresponded to high-quality-flagged data.

Reliable temperature profiles, a key issue for the retrieval of accurate CO columns, are difficult to obtain, as can be seen from Figure 5 which provides a set of different temperature profiles corresponding to the location and time of the img307 case. The three smooth profiles were calculated by meteorological models (ARPEGE,[50] ECMWF (European Centre for Medium-Range Weather Forecasts), and JMA [IMGDIS, IMG Level 2 data]). The two other profiles ([Payan[51]], [Serio[52]]) were directly retrieved from the IMG spectrum using the CO_2 absorption bands in IMG band 3.[49,53]

The temperature profiles as retrieved by Serio et al. were used in the inversion process to analyze the data, except for img921, referred hereafter as the WINCE (WINter Cloud Experiment) case, for which co-located radiosonde H_2O and temperature profiles were available.[35] Figure 6 illustrates the good agreement obtained in the CO absorption spectral range between a Level1C IMG radiance spectrum (img307) and the adjusted spectrum calculated by the LPMA global fitting procedure.

CO total column inversion results obtained from the participating groups are represented in Figure 7. Again, results are provided as relative differences (here $100\text{x}(CO_{inv}\text{-}CO_{avg})/CO_{avg}$, where CO_{avg}

is the mean value obtained from the averaging of all four results). It can be seen that discrepancies can be large, ranging from 17% difference between the two more distant results for the best case agreement (img822), to 37% for the worst case agreement (img906). The results obtained from the first part of this exercise on simulated spectra were used to analyze these discrepancies. Of the three parameters (noise, temperature profile and water vapor content) that were perturbed to check their associated impact on the retrieval accuracy, only the temperature profile was found to be less determined than what was used for the simulated spectra. Also, as already highlighted in previous papers, one of the major difficulties in the analysis of the IMG spectra is the lack of available information on the instrument line shape and ancillary geophysical parameters needed to invert CO, such as accurate co-located temperature profiles and information on cloud coverage.[40,49,54] These three sources of error were investigated.

3. Temperature profile

Specific tests were performed using the LPMA retrieval algorithm on the img307 case, fed with different temperature profiles (i.e. the profiles provided in Figure 5). It was found that differences between the CO columns obtained from the same algorithm using different temperature profiles can reach 25%. In all cases, the algorithms that can adjust the surface temperature parameter, to eventually compensate for an unknown surface emissivity and/or surface temperature were allowed to fit this parameter. Discrepancies of a few K between the initial surface temperature (provided by the first level of retrieved temperature profile) and the fitted value were found, reaching 10K for img304.

4. Instrument line shape

The LPMA algorithm has been used to perform various simulations in order to assess the impact of an incomplete knowledge of the instrument line shape on retrieved CO column amounts. Several

retrievals have been performed using different ILS, and the relative differences between the retrieved CO columns reached 18%. As each algorithm uses its own spectral range and minimization scheme, the impact of an incorrect instrument line shape for IMG data analysis is variable.

5. Cloud cover

An other source of discrepancy could come from the cloud coverage. Indeed, the retrieval of temperature was performed using IMG band 3 data (where CO_2 absorption bands occur), whereas CO retrievals were performed in band 2 where lines of the 1-0 fundamental transition occur. These two bands correspond to two adjacent footprints, separated by a 12 km distance. Therefore, one pixel may be affected by the presence of cloud and the other not, which impacts either the temperature profile or the CO retrieved concentration. All the IMG band 2 cases studied were documented as cloud-free in the CO spectral range in previous studies.[35,49,54] But at least the band 3 corresponding pixel for img307 was identified as 'possibly cloudy'.[52]

5. Conclusions

The forthcoming launch of polar-orbiting and geostationary spacecraft with instruments that will sound the troposphere will greatly enlarge our knowledge and understanding of the global CO distribution, a key compound to investigate the tropospheric oxidation budget. Modern remote sounders are expected to provide CO column amounts with at least 10 % accuracy, and possibly valuable vertical profiles with the help of data assimilation techniques.[55,56] The analysis of the radiance thermal channels provided by the IMG instrument on ADEOS,[41,56] and by the MOPITT instrument currently flying on EOS-TERRA, has already demonstrated the usefulness of nadir infrared soundings for the study of CO on the global scale.

This paper examined four L2 inversion algorithms currently under development for the inversion of CO total columns from nadir upwelling radiances provided by MOPITT, TES, and IASI. This

exercise generated useful interactions between the teams involved, to share experience and discuss specific problems, allowing us to improve our algorithms. Among other issues, we examined the channels used for the CO retrieval, the way the shape of the first guess profile is modified in the adjustment procedure, and the impact of inaccurate surface temperature and emissivity parameters. We have tried to show that all four algorithms performed well on simulated radiances, when ancillary data like instrumental noise, temperature profile and water vapor content are known with a reasonable accuracy. The accuracy of 1 K/1 km in the troposphere, which should be reached for temperature profiles retrieved with the TES and IASI instruments, was shown to be adequate for accurate CO retrievals.

This exercise was also useful in make us aware of unexpected difficulties when analyzing real atmospheric data. When data recorded by the IMG instrument were analyzed, the discrepancies between the different inversion results increased and proved to be much more difficult to analyze. Divergences were attributed to the lack of information regarding the IMG instrument line shape, the difficulty in using pixels that may exhibit different degrees of cloudiness for temperature and CO retrieval, and to the unavailability of accurate temperature profiles. The IMG team is working on improvement of the instrument line shape.[57] For current analyses of IMG data, we recommend convolving the IMG spectra with an apodization function to overcome this problem (e.g. Norton-Beer weak apodization function of 0.1 cm^{-1} FWHM for band 2).

Accurate trace gas retrievals rely first on efficient forward radiative transfer codes and associated spectroscopic parameters, which are continually improved through the spectroscopic databases used worldwide. Second, well-defined instrumental characteristics (noise, instrument line shape) are needed. Third, reliable ancillary parameters (temperature, other gas profiles, cloud contamination) are also required. For both the TES and IASI missions, coincident improved retrievals of temperature (surface and atmospheric profile) and cloud coverage information should be available

from the same instrument and within the same FOV as the one used for the CO retrieval, which should minimize the propagation of incorrect determination of these parameters in the CO retrieval. Large amounts of new data will become available from upcoming satellite missions. To fully exploit the atmospheric data to be provided by different kinds of instruments, the scientific community should combine those datasets, e.g. for trends and global change issues.[58] Each instrument team is developing its own algorithm, adapted to each instrument's constraints and design. This exercise was a first step towards the analysis of a common set of infrared nadir radiances. The dataset that was generated for this study is available upon request (ccl@aero.jussieu.fr). Work is continuing in the refinement of each retrieval scheme, e.g. to retrieve CO vertical profiles and other trace gases like O_3 and CH_4.[37,59]

Acknowledgements

The authors are very grateful to IMGDIS/ERSDAC for making the Level 1C IMG data available to us. We thank C. Serio for providing temperature profiles used in this study, P. Prunet for providing the IASI temperature error covariance matrix, and F. Karcher (Meteo-France) for the ARPEGE temperature profile. A. Goldman, B. Sen, and the two anonymous reviewers are acknowledged for their valuable comments on this manuscript. This work was undertaken in the framework of the ISSWG (IASI Sounding Science Working Group) activities under the auspices of EUMETSAT (European Organisation for the Exploitation of Meteorological Satellites) and CNES (Centre National d'Etudes Spatiales). The National Center for Atmospheric Research is sponsored by the National Science Foundation.

References

1. "World Meteorological Organization (WMO), Global Ozone Research and Monitoring Project, Scientific assessment of ozone depletion: 1998", *Rep.* **44**, Geneva (1999).

2. "Climate Change 2001: The Scientific Basis, Contribution of working group I to the third assessment report of the Intergouvernmental Panel on Climate Change," edited by J. T. Houghton, Y. Ding, D. J. Griggs, M. Noguer, P. J. van der Linden, X. Dai, K. Maskell, and C. Maskell, Cambridge Univ. Press (2001).

3. H. G. Reichle Jr., V. S. Connors, J. A. Holland, W. D. Hypes, H. A. Wallio, J. C. Casas, B. B. Gormsen, M. S. Saylor, and W. D. Hesketh,"Middle and upper tropospheric carbon monoxide mixing ratios as measured by a satellite-borne remote sensor during November 1981," J. Geophys. Res., **91(D10)**, 10,865-10,887 (1986).

4. H. G. Reichle Jr., V. S. Connors, J. A. Holland, R. T. Sherrill, H. A. Wallio, J. C. Casas, E. P. Condon, B. B. Gormsen, and W. Seiler, "The distribution of middle tropospheric carbon monoxide during early October 1984," J. Geophys. Res., **95(D7)**, 9845-9856 (1990).

5. V. S. Connors, B. B. Gormsen, S. Nolf, and H. G. Reichle Jr.,"Spaceborne observations of the global distribution of carbon monoxide in the middle troposphere during April and October 1994," J. Geophys. Res., **104**, 21,455-21,470 (1999).

6. H. G. Reichle, B. E. Anderson, V. S. Connors, T. C. Denkins, D. A. Forbes, B. B. Gormsen, R. L. Langenfelds, D. O. Neil, S. R. Nolf, P. C. Novelli, N. S. Pougatchev, M. M. Roell, and L. P. Steele, "Space shuttle based global CO measurements during April and October 1994, MAPS instrument, data reduction and data validation," J. Geophys. Res., **104**, 21,443-21,454 (1999).

7. C. P. Rinsland, M. R. Gunson, R. Zander, and M. Lopez-Puertas, "Middle and upper atmosphere pressure-temperature profiles and the abundances of CO_2 and CO in the upper atmosphere from ATMOS/Spacelab 3 observations," J. Geophys. Res., **97(D18)**, 20,479-20,495 (1992).

8. H. Kobayashi, A. Shimota, K. Kondo, E. Okumura Y. Kameda, H. Shimoda, and T. Ogawa,"A high-throughput Fourier-transform infrared radiometer for nadir Earth observations," Appl. Opt., **38(33)**, 6801-6807 (1999).

9. H. Kobayashi, A. Shimota, C. Yoshigahara, I. Yoshida, Y. Uehara, and K. Kondo,"Satellite-borne high-resolution FTIR for lower atmosphere sounding and its evaluation," IEEE Trans. Geosci. and Remote Sens., **37**, 1496-1507 (1999).

10. J. R. Drummond, and G. S. Mand, "The measurement of pollution in the troposphere," J. Atmos. Oceanic Technol., **13**, 314-320 (1996).

11. D. P. Edwards, J. -L. Attié, J.-F. Lamarque, D. Ziskin, J. C. Gille, B. Khattatov, M. Deeter, M. Smith, J. Warner, G. L. Francis, C. Cavanaugh, L. Mayer, J. Chen, J. Drummond, G. Mand, Z. Yu, "MOPITT observations of enhanced CO concentrations over Africa due to biomass burning, " American Geophys. Union 2000 Fall Meeting, San Francisco, Ca (15-19 Dec 2000).

12. J.-L. Attié, J. Gille, M. Deeter, D. P. Edwards, B. Katthatov, J.-F. Lamarque, L. V. Lyjak, P. Novelli, M. W. Smith, J. Warner and D. Ziskin : Validation of CO retrievals from MOPITT instrument aboard Terra Satellite, EGS Conference, Nice, France, (25-30 March 2001).

13. H. H. Aumann, and C. Miller, "Atmospheric infrared sounder (AIRS) on the Earth Observing System," Advanced and next-generation satellites, H. Fujisaka and N. M. Sweeting, editors, Proceedings of SPIE vol. **2583**, 332-338 (1995).

14. R. Beer, T. A. Glavich, and D. M. Rider, "Tropospheric emission spectrometer for the Earth Observing System's Aura satellite," Appl. Opt., **40(15)**, 2356-2367 (2001).

15. F. Cayla, and P. Javelle, "IASI instrument overview," Advanced and next-generation satellites, H. Fujisaka and N. M. Sweeting, editors, Proceedings of SPIE vol. **2583**, 271-281 (1995).

16. C. Camy-Peyret, B. Bergquist, B. Galle, M. Carleer, C. Clerbaux, R. Colin, C. Fayt, F. Goutail, M. Nunes-Pinharanda, J. P. Pommereau, M. Hausmann, U. Platt, I. Pundt, T. Rudolph, C. Hermans, P. C. Simon, A. C. Vandaele, J. M. C. Plane and N. Smith, "Intercomparison of instruments for tropospheric measurements using differential optical absorption spectroscopy," J. Atmos. Chem., **23**, 51-80 (1996).

17. A. Goldman, C. Paton-Walsh, W. Bell, G. C. Toon, J.-F. Blavier, B. Sen, M. T. Coffey, J. W. Hannigan, and W. G. Mankin, "Network for the detection of stratospheric change Fourier transform infrared intercomparison at Table Montain facility, November 1996," J. Geophys. Res., **104,(D23)**, 30,481-30,503 (1999).

18. L. S. Rothman, C. P. Rindsland, A. Golman, S.T. Massie, D. P. Edwards, J.-M. Flaud, A. Perrin, C. Camy-peyret, V. Dana, J.-Y. Mandin, J. Schroeder, A. McCann, R. R. Gamache, R. B. Wattson, K. Yoshino, K. V. Chance, K. W. Jucks, L. R. Brown, V. Nemtchinov, and P. Varanasi, "The HITRAN molecular spectroscopic database and HAWKS: 1996 edition," J. Quant. Spectrosc. Radiat. Transfer, **60**, 5, 665-710 (1998).

19. R. G. Ellingson and Y. Fouquart, "The intercomparison of radiation codes in climate models: An overview," J. Geophys. Res., **96**, 8925-8927 (1991).

20. S. A. Tjemkes, T. Patterson, R. Rizzi, M. W. Shephard, S. A. Clough, M. Matricardi, J. Haigh, M. Höpfner, S. Payan, A. Trotsenko, N. Scott, P. Rayer, J. Taylor, C. Clerbaux, L. L. Strow, S. DeSouza-

Machado, D. Tobin, and R. Knuteson, "ISSWG Line-by-line Intercomparison Experiment", J.Q.S.R.T., submitted for publication.

21. C. D. Rodgers, "Retrieval of atmospheric temperature and composition from remote measurements of thermal radiation," Rev. Geophys., **14(4)**, 609-624 (1976).

22. U. Amato, I. De Feis, and C. Serio, "Linearization pseudo-noise and its effect on the retrieval of atmospheric state from infrared spectral radiances," Geophys. Res. Letters, **23(18)**, 2565-2568 (1996).

23. B. Schimpf and F. Schreier, "Robust and efficient inversion of vertical sounding atmospheric high-resolution spectra by means of regularization, " J. Geophys. Res., **102(D13)**, 16037-16055 (1997).

24. P. Eriksson, "Analysis and comparison of two linear regularization methods for passive atmospheric observations," J. Geophys. Res., **105(D14)**, 18,157-18,167 (2000).

25. C. D. Rodgers, "Inverse methods for atmospheric sounding: Theory and practice," Series on Atmospheric, Oceanic and Planetary physics, **2**, World Scientific (2000).

26. M. T. Chahine, "Inverse problems in radiative transfer: A determination of atmospheric parameters," J. Atmos. Sci., **27**, 960-967 (1970).

27. W. L. Smith, H. M. Woolf, and H. E. Revercomb,"Linear simultaneous solution for temperature and absorbing constituent profiles from radiance spectra," Appl. Opt., **30(9)**, 1117-1123 (1991).

28. S. A. Clough, C. P. Rinsland, and P. D. Brown, " Retrieval of tropospheric ozone from simulations of nadir spectral radiances as observed from space," J. Geophys. Res., **100**, 16,579-16,593 (1995).

29. W. W. McMillan, L. L. Strow, B. G. Doddridge, W. L. Smith, H. E. Revercomb, and H. L. Huang, "Retrieval of carbon monoxide column densities using AIRS on EOS: validation of a prototype retrieval algorithm," Proc. SPIE, Int. Soc. Opt. Eng., **2830**, 169-179 (1996).

30. H. Worden, R. Beer, and C. Rindsland, "Airborne infrared spectroscopy of 1994 western wildfires," J. Geophys. Res., **102(D1)**, 1287-1299 (1997).

31. D. P. Edwards, C. M. Halvorson, and J. C. Gille ,"Radiative transfer modeling for the EOS Terra satellite Measurement of Pollution in the Troposphere (MOPITT) instrument," J. Geophys. Res., **104(D14)**, 16,755-16,775 (1999).

32. L. Pan, J. C. Gille, D. P. Edwards, P. L. Bailey, and C. D. Rodgers, "Retrieval of tropospheric monoxide for the MOPITT experiment," J. Geophys. Res., **103 (D24)**, 32,277-32,290 (1998).

33. J. Wang, J. C. Gille, P. L. Bailey, L. Pan, D. Edwards, and J. R. Drummond,"Retrieval of Tropospheric Carbon Monoxide Profiles from High-Resolution Interferometer Observations: A New Digital Gas Correlation (DGC) Method and Applications," J. Atmos. Sci., **56**, 219-232 (1999).

34. J. Wang, J. C. Gille, P. L. Bailey, J. R. Drummond, and L. Pan,"Instrument sensitivity and error analysis for the remote sensing of tropospheric carbon monoxide by MOPITT," J. Atmos. Oceanic Technol., **16**, 465-474 (1999).

35. J. Wang, J. Gille, H. Revercomb, and V. Walden, "Validation study of the MOPITT retrieval algorithm: Carbon monoxide retrieval from IMG observations during WINCE," J. Atmos. Oceanic Technol, **17**, 1285-1295, (2000).

36. "Level 2 Algorithm Theoretical Basis Document," Rep. JPL D-16474, Jet Propulsion Laboratory,

Pasadena, California, (1999). Also available from http://tes.jpl.nasa.gov/.

37. M. Luo, R. Beer, D. J. Jacob, J. A. Logan, and C.D. Rodgers, "Simulated observation of tropospheric ozone and CO with the Tropospheric Emission Spectrometer (TES) satellite instrument," J. Geophys. Res., to be published.

38. S. Payan, C. Camy-Peyret, P. Jeseck, T. Hawat, G. Durry, and F. Lefèvre ,"First direct simultaneous HCl and $ClONO_2$ profile measurements in the Arctic vortex," Geophys. Res. Lett., **25**, 2663-2666 (1998).

39. M. Carlotti,"Global fit approach to the analysis of limb-scanning atmospheric measurements," Appl. Opt., **27(15)**, 3250-3254 (1988).

40. C. Clerbaux, J. Hadji-Lazaro, S. Payan, C. Camy-Peyret and G. Mégie, "Retrieval of CO columns from IMG/ADEOS spectra," IEEE Trans. Geosci. and Remote Sens., **37,3**, 1657-1662 (1999).

41. J. Hadji-Lazaro, C. Clerbaux, and S. Thiria, "An inversion algorithm using neural network to retrieve atmospheric CO concentrations from high-resolution nadir radiances," J. Geophys. Res., **104(D19)**, 23,841-23,854 (1999).

42. J.-F. Müller, and G. Brasseur,"IMAGES: A three-dimensional chemical transport model of the global troposphere," J. Geophys. Res., **100**, 16,445-16,490 (1994).

43. C. Clerbaux, P. Chazette, J. Hadji-Lazaro, G. Mégie, J.-F. Müller, and S. A. Clough,"Remote sensing of CO, CH_4, and O_3 using a space-borne nadir-viewing interferometer," J. Geophys. Res., **103(D15)**, 18,999-19,013 (1998).

44. C. Clerbaux, J. Hadji-Lazaro, S. Payan, C. Camy Peyret, and J. Wang ,"Intercomparison of inversion

algorithms for the retrieval of CO from IMG/IASI ," Proceedings of the 8th International Workshop on Atmospheric Science from Space using Fourier Transform Spectrometry (ASSFTS), MeteoFrance, Toulouse (1998).

45. S. A. Clough, and M. J. Iacono, "Line-by-line calculation of atmospheric fluxes and cooling rates, 2, Application to carbon dioxide, ozone, methane, nitrous oxide, and the halocarbons," J. Geophys. Res., **100**, 16,519-16,535 (1995).

46. G. P. Brasseur, D.A. Hauglustaine, S. Walters, P. J. Rasch, J.-F. Müller, C. Granier, and X. X. Tie, "MOZART, a global chemical transport model for ozone and related chemical tracers, 1, Model description," J. Geophys. Res., **103(D21)**, 28,265-28,289 (1998).

47. D. A. Hauglustaine, G. P. Brasseur, S. Walters, P. J. Rasch, J.-F. Müller, L. K. Emmons and M. A. Carroll, "MOZART, a Global Chemical Transport Model or Ozone and Related Chemical Tracers, Part 2. Model Results and Evaluation," J. Geophys. Res., **103(D21)**, 28,291-28,335 (1998).

48. S. Payan (Laboratoire de Physique Moléculaire et Applications, Paris, France) and J. Hadji-Lazaro (Service d'Aéronomie, Paris, France), Private communication (1998).

49. A. M. Lubrano, C. Serio, S. A. Clough, and H. Kobayashi, "Simultaneous inversion for temperature and water vapor from IMG radiances," Geophys. Res. Lett, **27(16)**, 2533-2536 (2000).

50. F. Karcher (MétéoFrance, Toulouse, France), Private communication (1998).

51. S. Payan (Laboratoire de Physique Moléculaire et Applications, Paris, France), Private communication (1998).

52. C. Serio (Universita di Basilicata, Italy), Private communication (1999).

53. U. Amato, V. Cuomo, I. De Feis, F. Romano, C. Serio, and H. Kobayashi, "Inverting for geophysical parameters from IMG radiances," IEEE Trans. Geosci. and Remote Sens. **37**, 1620-1632 (1999).

54. J. Hadji-Lazaro, C. Clerbaux, P. Couvert, P. Chazette, and C. Boonne,"Cloud filter for CO retrieval from IMG infrared spectra using ECMWF temperatures and POLDER cloud data," Geophys. Res. Lett., **28(12)**, 2397-2400 (2001).

55. J. -F. Lamarque, B. V. Khattatov, J. C. Gille, and G. P. Brasseur,"Assimilation of Measurement of Air Pollution from Space (MAPS) CO in a three-dimensional model," J. Geophys. Res., **104**, 26,209-26,218 (1999).

56. C. Clerbaux, J. Hadji-Lazaro, D. Hauglustaine, G. Mégie, B. Khattatov, and J.-F. Lamarque, "Assimilation of carbon monoxide measured from satellite in a three-dimensional chemistry-transport model," J. Geophys. Res., **106(D14)**, 15,385-15,394 (2001).

57. S. Ichizawa, K. Kondo, M. Suzuki, H. Shimoda and T. Ogawa, "Improvement of the instrument line shape of IMG," Infrared Spaceborne Remote Sensing IX, M. Strojnik and B. F. Andresen, editors, Proceedings of SPIE Vol. **4486**, 326-334 (2002).

58. J. E. Harries, H. E. Brindley, P. J. Sagoo, and R. J. Bantges, "Increases in greenhouse forcing inferred from outgoing longwave radiation spectra of the Earth in 1970 and 1997," Nature, **410**, 355-357 (2001).

59. S. Turquety, J. Hadji-Lazaro, and C. Clerbaux, "Retrieval of ozone from infrared IASI measurements," Remote Sensing of Clouds and the Atmosphere VI, K. Schaefer, O. Lado-Bordowsky, A. Comeron, M. R. Carleer, J. S. Fender, editors, Proceedings of SPIE Vol. **4539**, 106-115 (2002).

Fig. 1. CO mixing ratio (total column amount=1.86x10^{18} molecule/cm^2) and temperature profiles used for the simulations. The solid and dashed lines correspond to the initial temperature profile and perturbed temperature profile, respectively.

Fig. 2. Nadir radiance (reference) spectrum simulated at 0.07 cm^{-1} spectral resolution in the CO absorption spectral range, for atmospheric conditions (top) and for CO alone (bottom).

Fig. 3. Radiance differences from the initial reference spectrum: case A is for noise added; case B corresponds to a perturbed temperature profile; case C combines the addition of noise and the temperature perturbation; case D corresponds to a perturbed water vapor profile.

Fig. 4. Relative deviation for CO total column retrieval from the reference case for each participating group. Case A is for noise added; case B corresponds to a perturbed temperature profile; case C combines the addition of noise and temperature perturbation; case D corresponds to a perturbed water vapor profile. Some results are provided with and without fitting of surface temperature (ST). The dashed line provides the standard accuracy expected for CO retrieval from infrared nadir radiances

Fig. 5. Temperature profiles as provided by 3 meteorological models and 2 retrieval algorithms for (-52.3^o longitude,41.0^o latitude) on June 16, 1997 (01H40 UT).

Fig. 6. IMG atmospheric spectrum (top), corresponding fit with the LPMA retrieval algorithm (middle), and difference between these two spectra (bottom) in the CO absorption spectral range.

Fig. 7. Relative deviation for CO total columns from the averaged value as retrieved by the participating groups using 5 selected IMG spectra. Averaged values in molecule/cm^2 are $1.50x10^{18}$, $1.77x10^{18}$, $1.64x10^{18}$, $1.78x10^{18}$, and $2.23x10^{18}$ for img304, img307, img822, img906 and img921, respectively (see Table 2 for recording times and locations).The dashed line provides the standard accuracy expected for CO retrieval from infrared nadir radiances

Table 1. Main characteristics of the CO retrieval algorithms

Characteristics	Digital Gas Correlation	TWPR	Global Fit	Neural Network
	NCAR	*JPL*	*LPMA*	*SA*
Instrument	MOPITT[10]	TES[14]	IASI[15]	IASI
Forward code	MOPFAS[31]	TWPR[36]	LPMA[38]	LBLRTM[45]
Atmospheric profiles	First guess	First guess	First guess	3D CTM[42]
Minimization algorithm	Maximum likelihood	Non-linear least squares	Levenberg-Marquardt	Gradient descent
Spectral range (cm^{-1})	2100-2250	2000-2250	2000-2185	132 selected channels[43]
Retrieved variables				
T_s/Emissivity	x	x	x	
CO	x	x	x	x
H_2O			x	
Time required[a]	$\sim$ 1sec	>10 min.	$\sim$ 10 min.	< 1sec

[a] for one spectrum inversion in 1999 (not representative of the current performance of each algorithm)

Table 2. IMG spectra

Name	IMG file	Long	Lat	Day/Month/Yr	hr:min:sec	Land/Sea	Elevation (m)
img307	432307	-52.3	41.0	16/06/97	01:40:01	S	0
img304	433304	60.1	24.5	16/06/97	18:24:33	S	0
img921	234921	-98.3	42.2	28/01/97	17:45:22	L	575
img906	327906	9.5	38.4	03/04/97	21:36:00	S	0
img822	372822	27.0	37.3	05/05/97	09:19:14	S	0

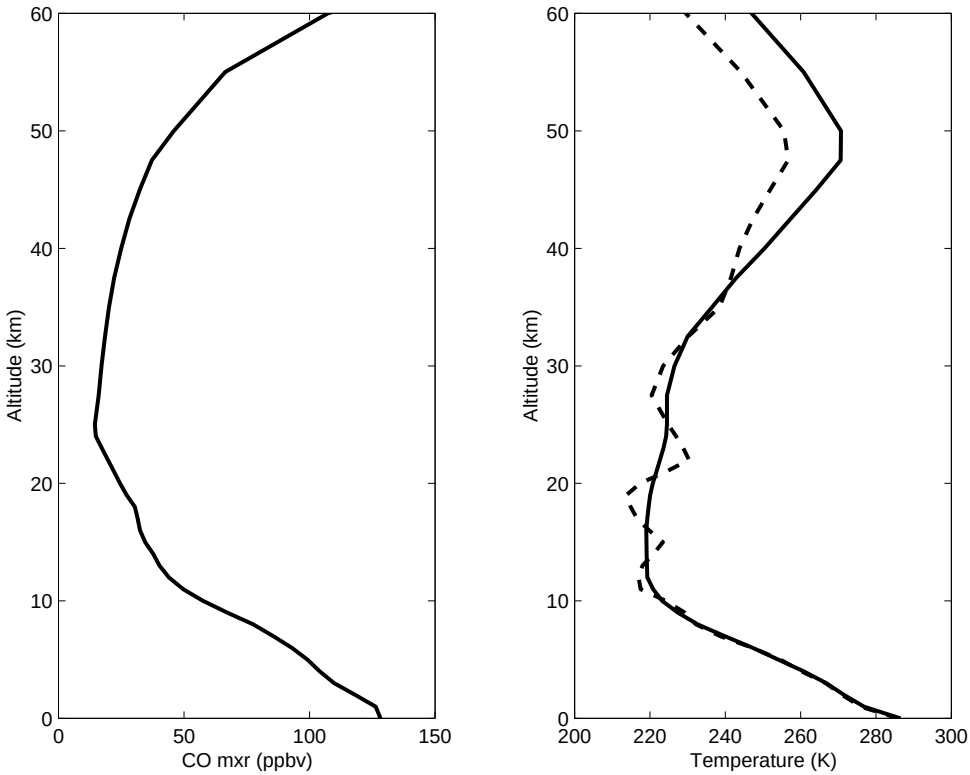

Figure 1, C. Clerbaux et al.

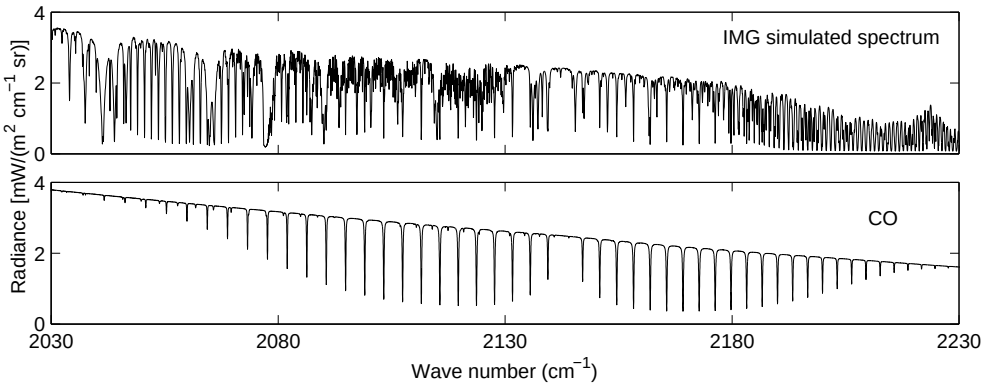

Figure 2, C. Clerbaux et al.

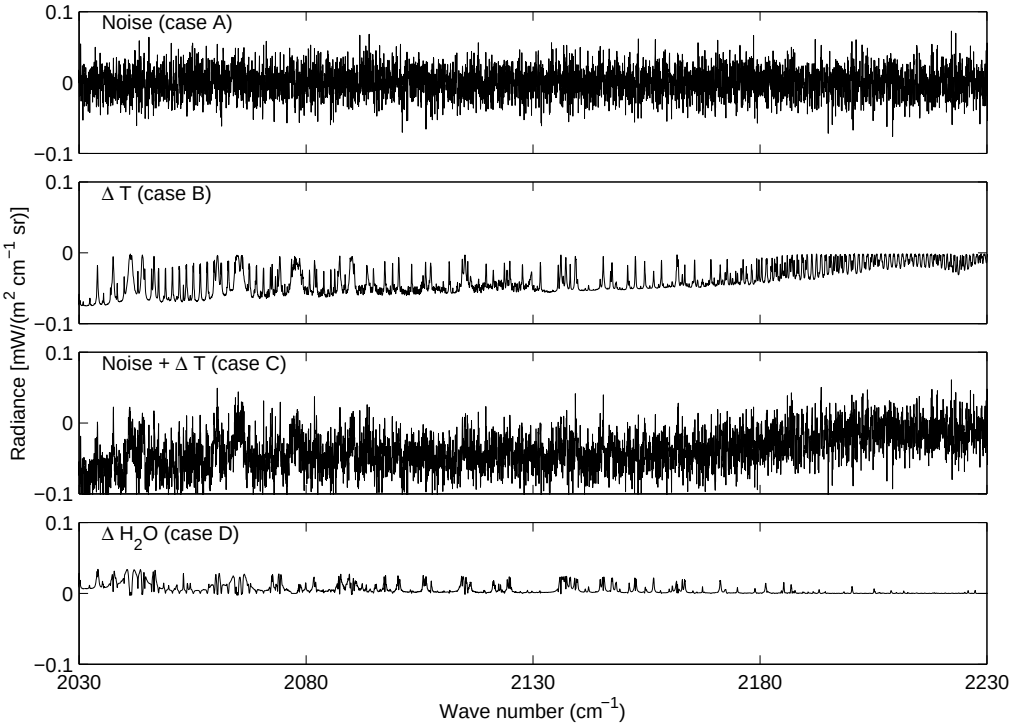

Figure 3, C. Clerbaux et al.

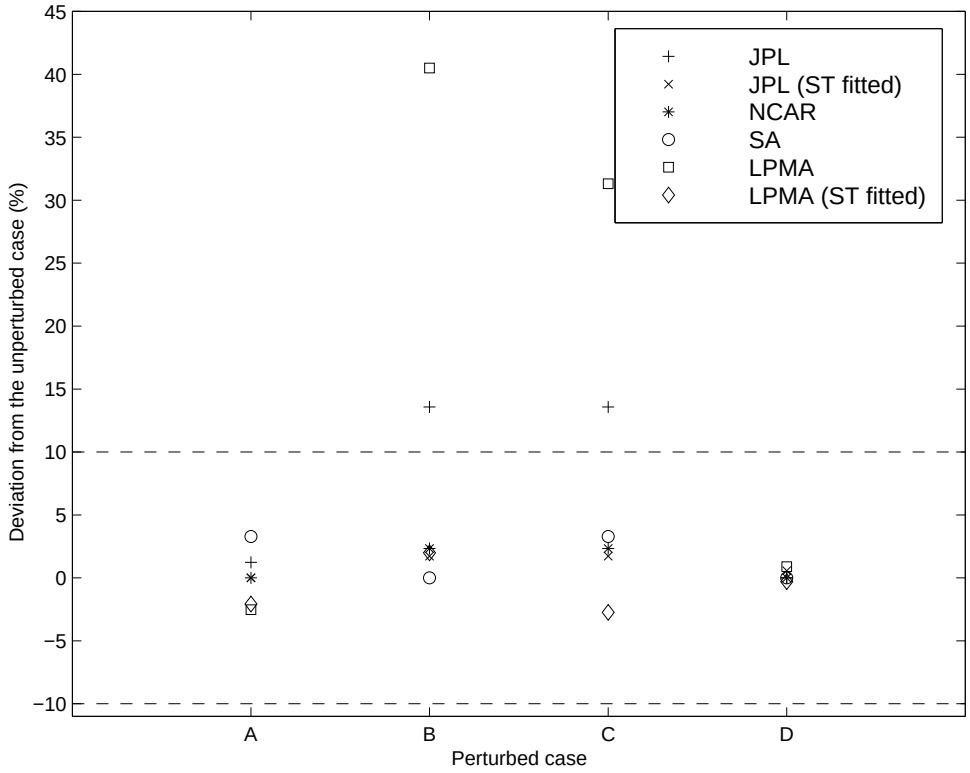

Figure 4, C. Clerbaux et al.

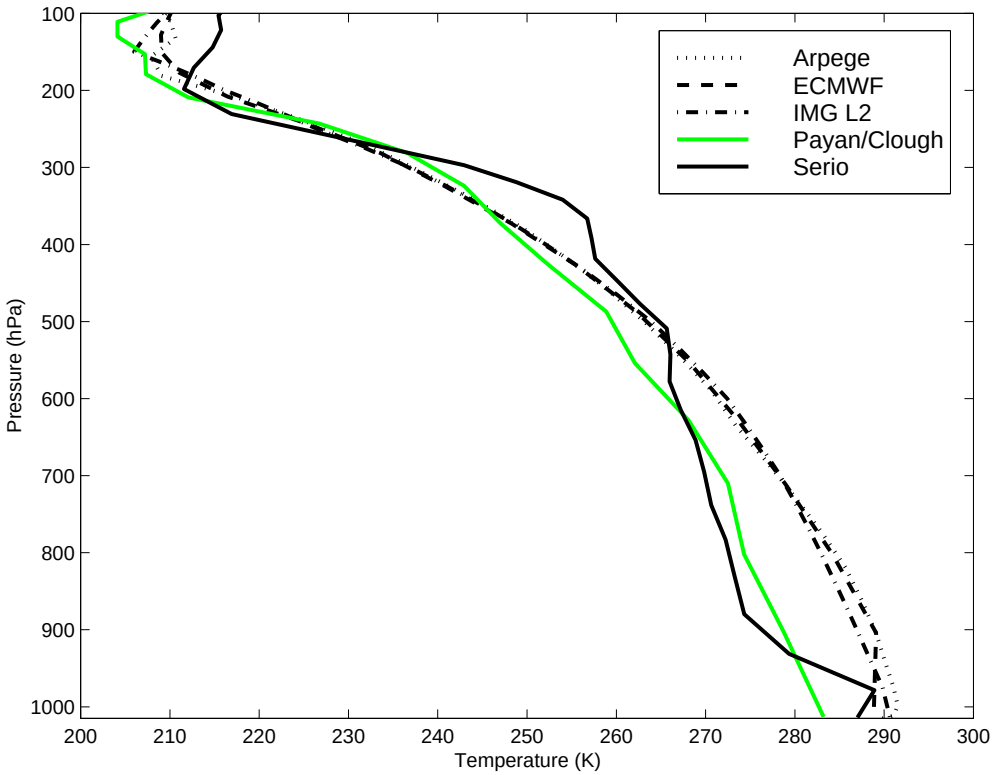

Figure 5, C. Clerbaux et al.

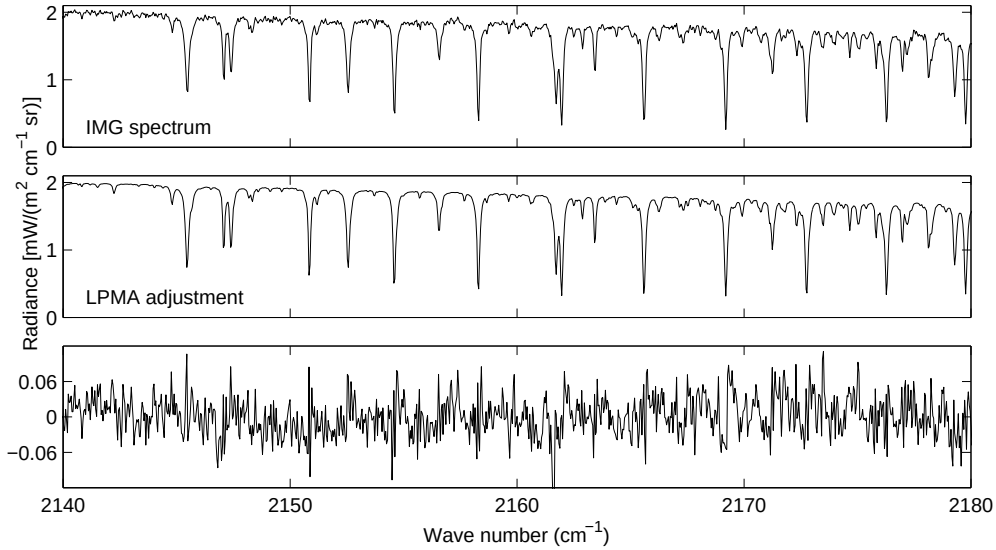

Figure 6, C. Clerbaux et al.

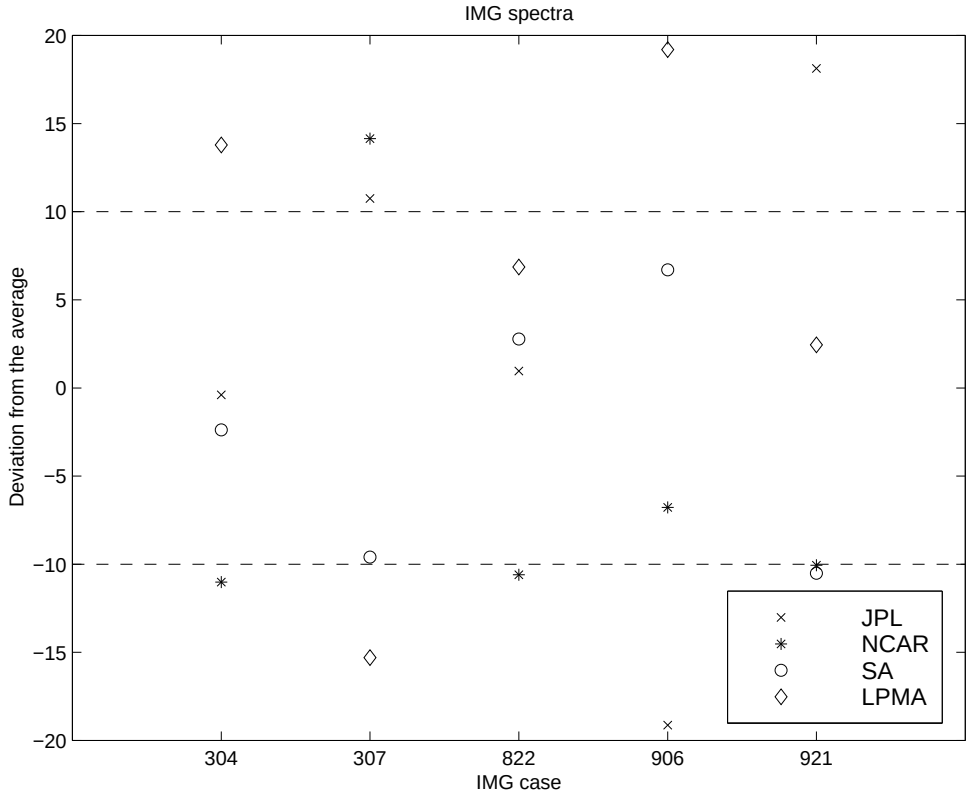

Figure 7, C. Clerbaux et al.